Scattering with absorptive interaction: Energy-dependent potentials

W. Cassing
Gesellschaft für Schwerionenforschung, 6100 Darmstadt, Federal Republic of Germany

M. Stingl
Institut für Theoretische Physik I, Universität Münster, 4400 Münster, Federal Republic of Germany

A. Weiguny*
Nuclear Theory Division, Los Alamos Scientific Laboratory, Los Alamos, New Mexico 87545
(Received 25 October 1982)

The energy dependence and analytic structure of the effective interaction for elastic scattering of composite particles are investigated using Feshbach's projection technique. A generalized Levinson theorem is established for complex, nonlocal, and energy-dependent interactions. The analytical results are illustrated by means of Argand diagrams for a solvable model and the effect of energy averaging is discussed.

[NUCLEAR REACTIONS Scattering theory, S matrix for absorptive, energy-dependent potentials, Levinson theorem.]

I. INTRODUCTION

In a previous paper[1] the partial-wave S matrix was studied for a wide class of complex interactions, both local and nonlocal. In particular, the motion of poles of the S matrix as a function of the absorptive strength of the interaction was examined, and approximations to the S matrix near resonances were deduced. In Ref. 1 both real and imaginary parts of the interaction were assumed to be energy independent; this assumption is not justified if one wants to cover a wide range of energies and to study threshold effects.

In the present paper, the energy dependence of the effective interaction in the elastic channel, resulting from a many-channel projection technique,[2] is investigated (Sec. II) and its influence on the Fredholm determinant and the S matrix are examined. On the basis of the analytic properties of the Fredholm determinant (Sec. III), a generalized Levinson theorem for the physical phase shift in the elastic channel is proven which takes into account the effects of channel coupling (Sec. IV). The general considerations of Secs. II—IV are tested and illustrated by a simplified two-channel model (Sec. V) which can be solved exactly. The results are represented in terms of Argand diagrams which are particularly suitable for displaying the analytic structure of the S matrix. With regard to experimental data, the influence of energy averaging is studied in a schematic ($N=30$)-channel calculation.

II. ENERGY DEPENDENCE OF THE EFFECTIVE INTERACTION BETWEEN COMPOSITE PARTICLES

Throughout this paper we shall restrict ourselves to a finite set of coupled two-body channels. In a nuclear-physics context, the model space is then spanned by wave functions Ψ_m of the type

$$\Psi_m = \phi_{\text{c.m.}} \mathscr{A}(\phi_m^A \phi_m^B g_m); \quad m = 1,2,\ldots,N \ , \tag{2.1}$$

where $\phi_{\text{c.m.}}$ describes the center-of-mass motion, ϕ_m^A and ϕ_m^B describe the internal fragment structures in channel m with the relative motion wave function g_m and $\mathscr{A}$ takes care of full antisymmetrization between the fragments. The Schrödinger equation in the above model space is equivalent to the following set of integrodifferential equations[3]

$$(T_{\rho m} + V_{mm} + \epsilon_m - E) g_m = -\sum_{m' \neq m} V_{mm'} g_{m'} \ . \tag{2.2}$$

$T_{\rho m}$ denotes the kinetic energy operator of relative motion in channel m, and ϵ_m the corresponding threshold energy. V_{mm} is the mean-field potential in channel m, which is coupled to channels $m' \neq m$ through the interactions $V_{mm'}$. Due to the antisymmetrization between the fragments, both V_{mm} and $V_{mm'}$ are nonlocal in the relative-motion coordinates ρ_m and $\rho_{m'}$. By preorthogonalization of the N chan-

nels under consideration, one can always ensure that V_{mm} and $V_{mm'}$ are independent of the total energy E of the two fragments in the c.m. system.

If one is only interested in elastic scattering in one specific channel, the projection technique of Feshbach[2] may be used to introduce an effective interaction in this particular channel. Let P denote the projector onto the channel of interest ($m=1$, say) and $Q=1-P$ the projector onto the remaining ("inelastic") channels of our model space. The effective Hamiltonian for the $m=1$ channel reads

$$H_{\text{eff}}=H_{11}+PHQ(E-QHQ)^{-1}QHP$$
$$=H_{11}+H_c(E)\ , \tag{2.3}$$

with

$$H_{11}=T_{\rho_1}+\epsilon_1+V_{11} \tag{2.4a}$$

and

$$H_c(E)=(V_{12}^* \cdots V_{1N}^*)\begin{bmatrix} E-H_{22} & \cdots & -V_{2N} \\ \vdots & & \vdots \\ -V_{N2} & \cdots & E-H_{NN}\end{bmatrix}^{-1}\begin{bmatrix} V_{12} \\ \vdots \\ V_{1N}\end{bmatrix}$$
$$:=V_c^\dagger G_Q V_c \tag{2.4b}$$

in obvious notation. Under appropriate restrictions on $V_{mm'}$ [cf. Ref. 1, Eqs. (2.5)], and noting that QHQ is a Hermitian operator in the Q subspace, G_Q may be expanded in the complete set of eigenstates of QHQ so that

$$H_c(E)=\sum_n \frac{V_c^\dagger|\phi_n\rangle\langle\phi_n|V_c}{E-E_n} + \lim_{\eta\to 0^+}\int_{\epsilon_2}^{\infty} d\epsilon \frac{V_c^\dagger|\phi_\epsilon\rangle\langle\phi_\epsilon|V_c}{E-\epsilon+i\eta}\ . \tag{2.5}$$

To prepare for the discussion of analytic properties and energy dependence of H_c we rewrite Eq. (2.5) as

$$H_c(E)=\sum_n \frac{D_n}{E-E_n}+C(E)-i\pi B(E)\ , \tag{2.6}$$

with

$$D_n=\sum_{i,j\neq 1} V_{1i}^*|\phi_{ni}\rangle\langle\phi_{nj}|V_{1j}\ ,$$
$$C(E)=\sum_{i,j\neq 1}\mathscr{P}\int_{\min(\epsilon_i,\epsilon_j)}^{\infty} d\epsilon \frac{V_{1i}^*|\phi_{\epsilon,i}\rangle\langle\phi_{\epsilon,j}|V_{1j}}{E-\epsilon}\ , \tag{2.7}$$
$$B(E)=\sum_{i,j\neq 1}\theta(E-\min(\epsilon_i,\epsilon_j)) \times V_{1i}^*|\phi_{\epsilon,i}\rangle\langle\phi_{\epsilon,j}|V_{1j}\ .$$

In Eq. (2.7), ϕ_{ni} denote the components of the bound state ϕ_n of QHQ at energy E_n, whereas the continuum states ϕ_ϵ have components $\phi_{\epsilon,i}$, starting at their respective threshold energies ϵ_i.

Starting out from a real nucleon-nucleon force and from real wave functions Ψ_m, the operators

$$V_c^\dagger|\phi_n\rangle\langle\phi_n|V_c$$

and

$$V_c^\dagger|\phi_\epsilon\rangle\langle\phi_\epsilon|V_c$$

are real. Moreover, they are non-negative since, e.g.,

$$\langle\alpha|V_c^\dagger|\phi_\epsilon\rangle\langle\phi_\epsilon|V_c|\alpha\rangle=|\langle\alpha|V_c^\dagger|\phi_\epsilon\rangle|^2\geq 0 \tag{2.8}$$

for an arbitrary diagonal element. Equation (2.8) ensures that $B(E)$ describes flux absorption rather than production. For example, a diagonal term of $C(E)$,

$$C_{ii}(E)=\mathscr{P}\int_{\epsilon_i}^{\infty}\frac{V_{1i}^*|\phi_{\epsilon i}\rangle\langle\phi_{\epsilon i}|V_{1i}}{E-\epsilon}d\epsilon\ , \tag{2.9}$$

is negative definite for $E<\epsilon_i$ and positive definite for sufficiently large E. Its general energy dependence is shown schematically in Fig. 1. Summation over indices i and j will lead to a smooth energy dependence of $C(E)$ below the first and above the Nth inelastic thresholds, while between these thresholds $C(E)$ may vary rapidly. Below the first inelastic threshold, the coupling to inelastic channels, $m=2,\ldots,N$, causes an additional attractive force which can give rise to additional bound states in the elastic ($m=1$) channel.

If there are any bound states of $H_Q:=QHQ$, the coupling Hamiltonian H_c becomes singular, giving rise to the well-known compound resonances.[2] Its

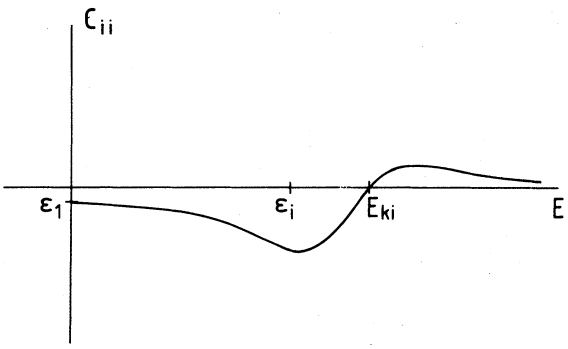

FIG. 1. Energy-dependence for a typical term in the real part of the coupling Hamiltonian H_c.

energy dependence can be studied analytically for separable interactions. For demonstration we have chosen the interactions to be of a Yamaguchi type,

$$V_{mm'}=\beta_{mm'}\frac{e^{-a_m\rho}}{\rho}\frac{e^{-a_{m'}\rho'}}{\rho'}\ , \tag{2.10}$$

and restricted ourselves to a two-channel problem. In this case $H_Q=H_2$ is a one-channel Hamiltonian,

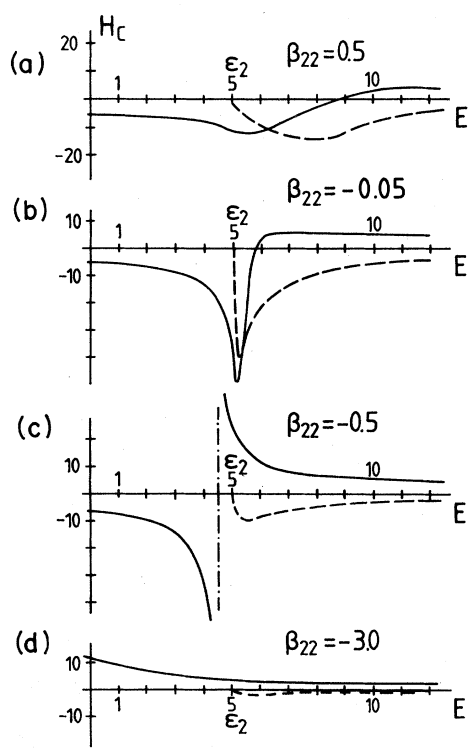

FIG. 2. Energy-dependence of the coupling Hamiltonian H_c (full line: real part; broken line: imaginary part) for various coupling strength β_{22} in a two-channel model (arbitrary units).

determined by the range parameter a_2 and the strength parameter β_{22}, and the coupling Hamiltonian H_c has the following form in momentum representation:

$$\frac{\gamma_1[k_2{}^2(E)]}{(k_1'^2+a_1{}^2)(k_1{}^2+a_1{}^2)},\quad k_2{}^2(E)=\frac{2\mu_2}{\hbar^2}(E-\epsilon_2)\ . \tag{2.11}$$

Figures 2(a)—(d) show the real and imaginary parts of γ_1 as a function of E for various values of the strength parameter β_{22}.

In Fig. 2(a) the interaction in channel $m=2$ is assumed to be repulsive ($\beta_{22}>0$). Hence there is no bound state of H_2, and $\mathrm{Re}\gamma_1$ shows the same structure as C_{ij} in Fig. 1. For attractive forces the situation changes drastically: As soon as β_{22} becomes negative, a compound resonance[2] may appear just beyond the threshold ϵ_2. This causes a rapid change of $\mathrm{Re}\gamma_1$ and a sharp increase of $\mathrm{Im}\gamma_1$ [Fig. 2(b)], according to Eq. (2.7), since the modulus of $\phi_{\epsilon,i}$ becomes large in the vicinity of a resonance. With β_{22} decreasing further, H_2 will develop a bound state between the thresholds. This leads to [see Fig. 2(c)] a pole of $\mathrm{Re}\gamma_1$ while $\mathrm{Im}\gamma_1$ is reduced as compared to Fig. 2(b) as long as no further resonance appears. Finally, H_2 can have a bound state below the first threshold ϵ_1 [see Fig. 2(d)], causing the effective interaction in channel 1 to be repulsive for $E>\epsilon_1$. In contrast to the cases displayed in Figs. 2(b) and (c), the corresponding pole of H_c for $E<\epsilon_1$ does not influence the physical phase shift through the generalized Levinson theorem, as we shall see in Sec. IV.

III. ANALYTIC PROPERTIES OF THE EFFECTIVE INTERACTION BETWEEN COMPOSITE PARTICLES

Let us start from a simple example by studying a separable, energy-dependent interaction given in momentum space as

$$\langle\vec{p}\,|\,V\,|\,\vec{p}\,'\rangle=g(E)\sum_l f_l(p)f_l^*(p')\times P_l(\hat{p}\cdot\hat{p}\,')\frac{2l+1}{4\pi pp'} \tag{3.1}$$

with a singularity in the coupling constant at $E=E_0$,

$$g(E)=g_0+\alpha^2/(E-E_0)\ . \tag{3.2}$$

Since for a separable operator B

$$\det(1-B)=1-\mathrm{Tr}B\ , \tag{3.3}$$

the Fredholm determinant[4] for the $l=0$ partial wave

$$d_0(g,k)=\det(1-G_0^0(k)V_0) \tag{3.4}$$

is easily seen to have the explicit form ($E=k^2/2\mu$)

$$d_0(g,k)=1-g(k^2)\int_0^\infty \frac{|f_0(p)|^2dp}{(k^2-p^2)+i0^+} . \tag{3.5}$$

The energy dependence of the coupling constant g changes the overall analytic structure of d_0 with respect to k. None of the poles and zeros of d_0 are where they would be if g were taken to be a constant. The primary effect, however, consists of introducing a pole of the Fredholm determinant at $E=E_0$ as well as a zero at some (in general complex) energy

$$E_r=E_0+\Delta-\frac{i}{2}\Gamma .$$

According to the relation[1]

$$S_0(g,k)=\frac{d_0(g,-k)}{d_0(g,k)} \tag{3.6}$$

this zero implies a pole of the S matrix at $E=E_r$. For real energies $E<0$, d_0 is real by virtue of Eq. (3.5) so that, for $E_0+\Delta<0$, the above zero of d_0 lies on the (negative) *real* energy axis, i.e., $\Gamma=0$. If $E_0+\Delta>0$, the zero lies in the right half of the complex energy plane where d_0 is complex, implying a nonzero $\Gamma>0$ since

$$\alpha^2|f_0(p)|^2>0 .$$

According to Eq. (3.6) this implies a resonance of S_0 which may come close to the real E axis provided $\alpha^2 \ll |g_0|$ ("compound resonance").

We shall now generalize the above results for the case of the effective interaction of Eq. (2.3),

$$V_{\text{eff}}=V_{11}+H_c(E) , \tag{3.7}$$

whose energy dependence is entirely determined by $G_Q(E)$, cf. Eq. (2.5). Inspection of Eqs. (2.6) and (2.7) shows that H_c is a meromorphic function of the channel momenta

$$\kappa_n=\left[\frac{2\mu_n}{\hbar^2}(E-\epsilon_n)\right]^{1/2}, \quad n=1,2,\ldots,N \tag{3.8}$$

for $\mathrm{Im}\kappa_n\geq 0$ provided the interactions $V_{nn'}$ are Hilbert-Schmidt kernels.[5] For $\mathrm{Im}\kappa_n>0$, i.e., on the "physical sheet," the relations

$$k=\left[\frac{\mu_1}{\mu_n}\kappa_n^2+\frac{2\mu_1}{\hbar^2}\epsilon_n\right]^{1/2}, \qquad n=1,2,\ldots,N \tag{3.9}$$

$$\kappa_n=\left[\frac{\mu_n}{\mu_1}k^2-\frac{2\mu_n}{\hbar^2}\epsilon_n\right]^{1/2},$$

constitute an analytic mapping except for branch points at

$$k_n=\pm\left[\frac{2\mu_1}{\hbar^2}\epsilon_n\right]^{1/2} . \tag{3.10}$$

Hence, the coupling Hamiltonian H_c is a meromorphic function of k for $\mathrm{Im}k\geq 0$ apart from branch points at real values

$$k_n=\pm(2\mu_1\epsilon_n/\hbar^2)^{1/2} ,$$

and has poles at

$$k_i=\pm(2\mu_1E_i/\hbar^2)^{1/2}$$

according to Eq. (2.6). The Green's function in the "elastic" channel,

$$G_1=(E-H_{11})^{-1} , \tag{3.11}$$

is a meromorphic function of k for $\mathrm{Im}k>0$ and has poles at the eigenvalues of H_{11}, as well as a branch point at the elastic threshold.

The Fredholm determinant of the full effective interaction (3.7) is constructed, in direct analogy to Ref. 1, by defining the following kernels:

$$\begin{aligned} K&=G^0(V_{11}+H_c) ,\\ K_1&=G^0V_{11} ,\\ K_{1c}&=G_1H_c . \end{aligned} \tag{3.12}$$

Using the resolvent identity

$$G_1=G^0+G^0V_{11}G_1 \tag{3.13}$$

one finds directly the relation

$$K=K_1+K_{1c}-K_1K_{1c} , \tag{3.14}$$

or equivalently,

$$1-K=(1-K_1)(1-K_{1c}) . \tag{3.14'}$$

Hence the Fredholm determinants d, d_1, and d_{1c} corresponding to the kernels K, K_1, and K_{1c}, respectively, are connected through

$$d=d_1d_{1c} . \tag{3.15}$$

d_1 is an analytic function of k for $\mathrm{Im}k\geq 0$,[5] with zeros at the bound states and resonances of H_{11}, while d_{1c} is a meromorphic function of k having the same singularities as K_{1c}. According to Eq. (3.15), the zeros of d_1 will cancel those poles of d_{1c} which are due to G_1. The full Fredholm determinant d is, therefore, a meromorphic function of k for $\mathrm{Im}k\geq 0$ except for the branch points k_n [Eq. (3.10)] at the threshold energies; it has poles at the bound states of QHQ according to (2.6), and its zeros are the same as for d_{1c}. The possible positions of zeros and poles

of d are shown in Fig. 3. Note in particular the following:

(1) In accordance with the introductory example to this section, the bound states of QHQ at E_i give rise to *pairs* of poles and zeros of $d(k)$. If $\epsilon_1 < E_i < \epsilon_N$, the poles lie on the real k axis and the zeros (representing compound resonances) appear in the lower half of the k plane. For $E_i < \epsilon_1$, the poles appear on the imaginary axis with the associated zeros close by.

(2) The poles of $d(k)$ due to bound states of QHQ are located symmetrically with respect to the imaginary k axis, while the zeros of $d(k)$, corresponding to compound and potential resonances, lose that symmetry in the presence of the imaginary part of H_c (cf. the discussion in Ref. 1).

(3) Nonlocal potentials may exhibit positive-energy bound states.[5] Such normalizable states embedded in the continuum show up as pairs of zeros of $d(k)$ on the real axis symmetrical to $k=0$. Depending on the choice of the model space, one may also have normalizable states which solve the dynamical equations (2.2) at arbitrary energy. Such "redundant" states, which are a consequence of the Pauli principle,[2,6] will not be discussed in the following. We refer the reader to Ref. 7. Furthermore, we assume, as in Ref. 1, that so-called "spurious states"[7] are absent.

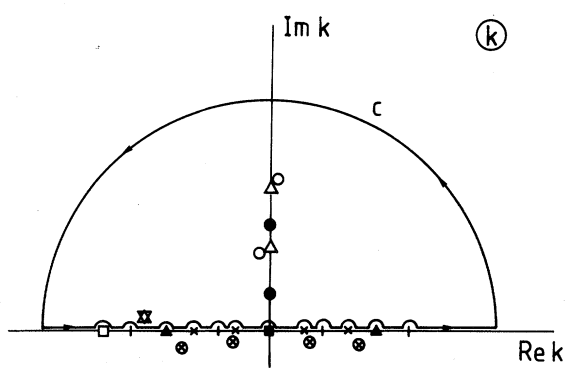

FIG. 3. Contour of integration C and possible positions of poles and zeros of the Fredholm determinant $d(k)$, relevant to the Levinson theorem. $\times$: poles of $d(k)$ for real k corresponding to bound states of QHQ for $\epsilon_1 < E < \epsilon_N$, appearing in pairs symmetrical to $k=0$. Their number, multiplied by their respective order, is denoted by n_Q. $\otimes$: zeros of $d(k)$ with $\mathrm{Im}k<0$ corresponding to compound resonances. $\square$: zeros of $d(k)$ corresponding to compound resonances or potential resonances, shifted onto the negative real k axis by $\mathrm{Im}H_c$. Their number, multiplied by the respective order, is denoted by n_R. ✡: zeros of $d(k)$ resulting from compound resonances or potential resonances, shifted into the second quadrant of the k plane through $\mathrm{Im}H_c$. Let n_I be their number, taking into account the respective order. $\triangle$: poles of $d(k)$ on the positive imaginary axis, due to the bound states of QHQ for $E<\epsilon_1$. Let n_{CS} be their number. $\circ$: zeros of $d(k)$ associated with a Δ pole. $\bullet$: zeros of $d(k)$ which correspond to bound states of H_{eff}. Their number is n_B. $\blacksquare$: possible zero of $d(k)$, of order q, at $k=0$ representing a zero-energy bound state of H_{eff}. $\blacktriangle$: positive energy bound states. Let n_P denote the number of such pairs. The energy scale is chosen such that $\epsilon_1=0$. Branch points are marked as $-\!\!+\!\!-$.

IV. A GENERALIZED LEVINSON THEOREM

We are now in a position to establish a generalized Levinson theorem for the phase shift $\delta(k)$ in the elastic ($m=1$) channel, taking into account the effects of channel coupling. We shall restrict ourselves to spin-zero fragments, so that the relative orbital angular momentum is a conserved quantity; to simplify the notation we shall suppress the corresponding index l throughout this section. The proof of the theorem will rest on the analytic properties of $d(k)$, as discussed in the preceding section, and on the asymptotic behavior of $d(k)$,[5]

$$\begin{matrix} d(k)\to 1\ , \\ \dfrac{d}{dk}(\ln d(k))\to 0\ , \end{matrix} \quad \text{for } |k|\to\infty\ . \tag{4.1}$$

Special care is required in relating the argument of $d(k)$ to the (negative) physical phase shift $\delta(k)$ since, in the general case, $d(k)$ may have zeros and poles on the real k axis, and $\arg d(k)$ is not antisymmetric with respect to k (Ref. 1), in contrast to $\delta(k)$. We proceed in a similar way as in Ref. 1 and start by replacing $d(k)$ by some other function which has the same zeros and asymptotic behavior and similar analytic properties as $d(k)$, but is antisymmetric in k. Except for discontinuities to be discussed below, this function will carry the negative physical phase shift.

To this end we define the following function, at least piecewise continuous:

$$\phi(k) = -\tfrac{1}{2}(\arg[d(k)] + \arg[d(-k^*)])\ , \tag{4.2}$$

which is zero for real interactions.[1] Moreover, we define a function $\tilde{d}(k)$ by a Jost-Kohn type of integral[8]

$$\tilde{d}(k) = \exp\left[\frac{1}{\pi}\int_{-\infty}^{\infty} dk' \frac{\phi(k')}{k'-k}\right]\ , \tag{4.3}$$

which is analytic outside the real k axis. Then

$$|\tilde{d}(k)| = \exp\left[\frac{1}{\pi}\mathscr{P}\int_{-\infty}^{\infty} dk' \frac{\phi(k')}{k'-k}\right] \neq 0 ,$$

$$\arg[\tilde{d}(k+i0)] = \phi(k) , \tag{4.4}$$

for real k, and $\phi(k) \to 0$ as $|k| \to \infty$, so that

$$\tilde{d}(k) \to 1 \text{ as } |k| \to \infty . \tag{4.5}$$

The function

$$\hat{d}(k) = d(k)\tilde{d}(k) \tag{4.6}$$

then has the same zeros, poles, and branch points as the original Fredholm determinant $d(k)$ and is meromorphic for $\mathrm{Im}k \geq 0$, except for the branch points, as is $d(k)$. The negative of its argument is

$$-\arg[\hat{d}(k)] = -\arg[d(k)] - \phi(k)$$
$$= \tfrac{1}{2}\{\arg[d(-k)] - \arg[d(k)]\} \tag{4.7}$$

for real k, which manifestly shows the desired antisymmetry. From (4.1) and (4.5) we obtain the asymptotic behavior

$$\begin{aligned} &\hat{d}(k) \to 1 , \\ &\frac{d}{dk}(\ln\hat{d}(k)) \to 0 , \end{aligned} \quad \text{for } |k| \to \infty . \tag{4.8}$$

We normalize $\ln\hat{d}(k=\infty)=0$.

We are now prepared to calculate

$$\arg[\hat{d}(\infty)] - \arg[\hat{d}(0)]$$

by evaluating the integral

$$I = \oint_C \left[\frac{d}{dk}\ln\hat{d}(k)\right] dk \tag{4.9}$$

along the contour C of Fig. 3. Applying the residue theorem, one obtains

$$I = 2\pi i(n_B - n_{CS} + n_{CS} + n_I) = 2\pi i(n_B + n_I) , \tag{4.10a}$$

bearing in mind that the residue of the logarithmic derivative of $\hat{d}(k)$ is determined by the negative order of a pole and the positive order of a zero, respectively. Thus the contributions from poles $(-n_{CS})$ and zeros $(+n_{CS})$ of $d(k)$ due to bound states of QHQ below ϵ_1 cancel in (4.10a). n_B denotes the number of bound states of H_{eff} and n_I the number of zeros of $d(k)$ resulting from compound and potential resonances shifted into the second quadrant of the k plane through $\mathrm{Im}H_c$. [In this context, by potential resonances we mean resonances of H_{11}, modified by contributions from $C(E)$, Eq. (2.7).] If (4.9) is evaluated directly as a line integral, there are no contributions from the large semicircle by virtue of (4.8), and the contributions of the small semicircles around zeros, poles, and branch points of $\hat{d}(k)$ at real k cancel the jumps of $\arg\hat{d}(k)$ at these points, so that

$$I = 2i(\arg[\hat{d}(\infty)] - \arg[\hat{d}(0)]) \tag{4.10b}$$

using the antisymmetry of $\hat{d}(k)$, Eq. (4.7). Comparing the two results one has

$$\arg[\hat{d}(\infty)] - \arg[\hat{d}(0)] = \pi(n_B + n_I) . \tag{4.11}$$

Some care is required in relating the phase of $\hat{d}(k)$ to the physical phase shift $\delta(k)$ whenever $\hat{d}(k)$ has zeros or poles on the real k axis. To avoid ambiguities we define[9] the physical phase shift $\delta(k)$ in the elastic channel as half the phase of $S_{11}(k)$, continued downward in energy *without jumps of* π from a conventional value of $\delta(\infty)=0$. There are three cases to be considered, as shown schematically in Fig. 4:

(1) $\hat{d}(k)$ may have a pair of zeros at some real momenta $\pm k_0$ corresponding to a positive-energy bound state that happens to survive in the presence of $\mathrm{Im}H_c$. While $\delta(k)$ is continuous by definition, the phase of $\hat{d}(k)$ must *discontinuously drop* by π (Ref. 9) when k passes through $\pm k_0$ in the positive k direction. Therefore, in such a case,

$$\arg[\hat{d}(0)] - \arg[\hat{d}(\infty)] = -\delta(0) + \delta(\infty) + n_P\pi , \tag{4.12}$$

where n_P is the number of positive-energy bound states in the partial wave under consideration.

(2) Poles of $S_{11}(k)$ of the third quadrant, due to compound or potential resonances, may be shifted

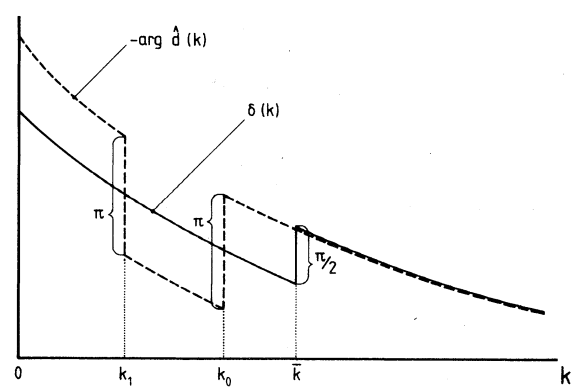

FIG. 4. Schematic representation of discontinuities in $-\arg\hat{d}(k)$ (dashed line) and $\delta(k)$ (full line) due, respectively, to one positive-energy bound state ($n_P=1$) at $k=k_0$, and one bound state of QHQ above elastic threshold ($n_Q=1$) at $k=k_1$ and one pole of $S(k)$ shifted onto the negative real k axis by the absorptive part of H_C ($n_R=1$). We assume $n_B=n_I=0$.

onto the negative real k axis through $\mathrm{Im}H_c$.[1] If such a pole has moved to $k=-\bar{k}$, $S_{11}(k)$ will have a zero at momentum $\bar{k}$ on the positive real k axis. When moving around this zero, in the direction of increasing k, the phase of $S_{11}(k)$ must *increase* by π.[10] Hence the physical phase shift $\delta(k)$ increases discontinuously by $\pi/2$, whereas the phase of $\hat{d}(k)$ changes in a continuous manner since both $d(\bar{k})$ and $\tilde{d}(\bar{k})$ are nonzero. Note that a jump by $\pi/2$ is allowed with our definition of the physical phase shift. Denoting the number of such poles by n_R, we have

$$\arg[\hat{d}(0)]-\arg[\hat{d}(\infty)]=-\delta(0)+\delta(\infty)-n_R\pi/2 \ . \tag{4.13}$$

(3) There are poles of $d(k)$ [or $\hat{d}(k)$, respectively] corresponding to bound states of QHQ with $\epsilon_1<E_i<\epsilon_N$ appearing in pairs symmetrical to $k=0$. When passing through such points $\pm k_i$ in the positive k direction, the phase of $\hat{d}(k)$ must *discontinuously increase* by π while $\delta(k)$ remains continuous with the above definition. Hence

$$\arg[\hat{d}(0)]-\arg[\hat{d}(\infty)]=-\delta(0)+\delta(\infty)-n_Q\pi \ , \tag{4.14}$$

where n_Q is the number of bound states of QHQ with $\epsilon_1<E_i<\epsilon_N$.

Combining Eqs. (4.11)–(4.14) gives the final result (cf. Fig. 4)

$$\delta(0)-\delta(\infty)=\pi(n_B+n_p+n_I-n_Q+[q-n_R]/2) \ , \tag{4.15}$$

where q denotes the order of a possible bound state of H_{eff} at zero energy. Equation (4.15) differs from the result obtained in Ref. 1 for energy-independent, complex potentials by including the number n_Q of bound states of QHQ with $\epsilon_1<E_i<\epsilon_N$. The negative sign is easily understood: The Levinson theorem reflects the dimension of the subspace inaccessible to a scattering system by orthogonality. On the other hand, the coupling of the elastic channel to the eigenstates of QHQ enlarges the space accessible for scattering; they are, therefore, counted in the Levinson theorem with a sign opposite to that for bound states.

In the *weak-coupling limit,* the imaginary part of H_c will be too small to shift resonances into the second quadrant or onto the negative real k axis. Hence

$$n_I=n_R=0 \ . \tag{4.16}$$

Similarly, the real part of H_c will not change the number of bound states in the elastic channel so that

$$n_B=n_B^0, \quad n_P=n_P^0 \ , \tag{4.17}$$

where the index zero refers to the bound states generated by V_{11} alone. Excluding the highly accidental case where H_{eff} has bound states at zero energy (i.e., assuming $q=0$), the Levinson theorem reduces to

$$\delta(0)-\delta(\infty)=\pi(n_B^0+n_P^0-n_Q) \quad \text{(weak coupling)} \ . \tag{4.18}$$

The number n_Q still appears in Eq. (4.18). Only if the P and Q spaces are totally decoupled does Eq. (4.18) reduce to the standard form of the Levinson theorem.

V. COUPLED CHANNEL PROBLEM IN AN EXACTLY SOLVABLE MODEL

In this section we illustrate and test the above general results with a simplified model which can be solved exactly. Following Weidenmüller[11] we assume that the potential matrix elements $V_{mm'}$ are local and constant within a finite range,

$$V_{mm'}(\rho,\rho') \begin{cases} =0 \text{ for } \rho,\rho'>a \ , \\ =-V_{mm'}\delta(\rho-\rho') \ \text{ for } \rho\le a \ . \end{cases} \tag{5.1}$$

Although this parametrization is a rather drastic simplification, it should be perfectly sufficient to study the basic analytic properties of the multichannel S matrix and to test the generalized Levinson theorem. Throughout the calculation the reduced mass was assumed to be the proton mass and the range of the interactions to be $a=2$ fm in all channels. The results of the calculation for various sets of potential parameters $V_{mm'}$ are presented in terms of Argand diagrams, which are particularly suitable for displaying the analytic structure of the S matrix.

Figures 5 and 6 show Argand diagrams for the two-channel problem for various values of V_{11}, V_{12}, and V_{22}. For easy orientation, the eigenvalues of a square-well potential, with range $a=2$ fm and for the proton mass, are listed in Table I for various potential depths. Figure 5(a) describes a situation where V_{11} is not strong enough to produce a bound state in channel 1, whereas V_{22} supports a bound state in channel 2 just below the threshold ϵ_2, which was chosen to be 10 MeV. The Argand graph starts moving counterclockwise on the unit circle up to about 2.8 MeV, indicating a weak resonance due to V_{11} directly beyond threshold ($\epsilon_1=0$). Having passed the resonance, the graph reverses its direction of motion until the bound state in channel 2 becomes important at about 5.8 MeV: Moving counterclockwise again it points to the corresponding compound resonance. At 10 MeV the second chan-

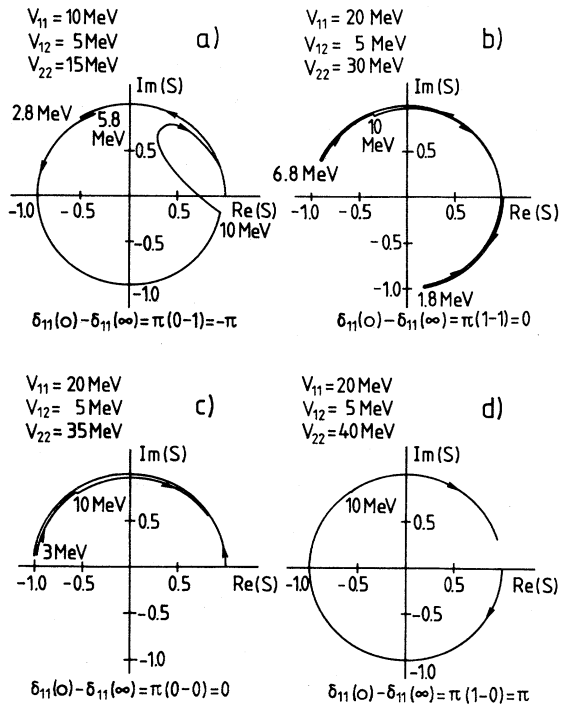

FIG. 5. Argand diagrams of the elastic-channel S matrix, resulting from a two-channel problem, for various sets of potential parameters in Eq. (5.1). The generalized Levinson theorem is exemplified for various values of the number of bound states n_B and compound resonances n_Q.

nel opens and the absolute value of S_{11} drops below 1 due to the imaginary part of H_c [cf. Fig.2 (c)], accounting for the loss of flux from channel 1 into

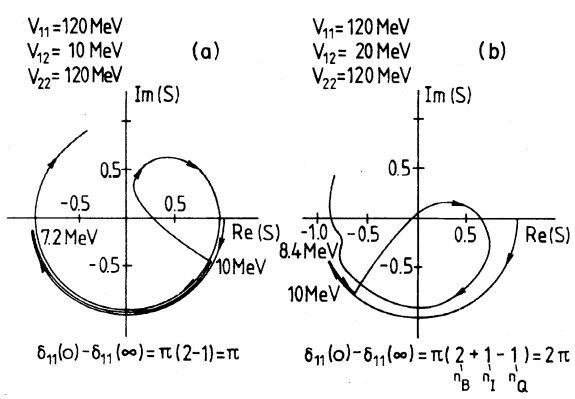

FIG. 6. Argand diagrams as in Fig. 5, showing the influence of the coupling V_{12} between the channels. In case (b) the coupling is strong enough to shift a resonance from the third into the second quadrant via the absorptive part of H_c.

TABLE I. Positions of bound states (E_B) in a square-well potential (range $a=2$ fm; reduced mass=proton mass) for various values of the potential depth V_0.

V_0 (MeV)	E_B (MeV)
5	
10	
12	
15	−0.207
20	−1.789
30	−7.361
33	−9.389
34	−10.090
35	−10.802
50	−22.441
80	−48.519
110	−76.169
120	−0.793 and −85.569
150	−17.263 and −114.569

channel 2. With the energy increasing further, the Argand graph tends to the point (1,0). Thus we have

$$\delta(0)-\delta(\infty)=-\pi$$

as expected from Eq. (4.15) in the presence of one compound resonance, caused by a bound state of V_{22} for $\epsilon_1<E<\epsilon_2$, and no bound state in the elastic channel (i.e., $n_Q=1$, $n_B=0$). Cases (b)—(d) in Fig. 5 refer to a system with one bound state in the elastic

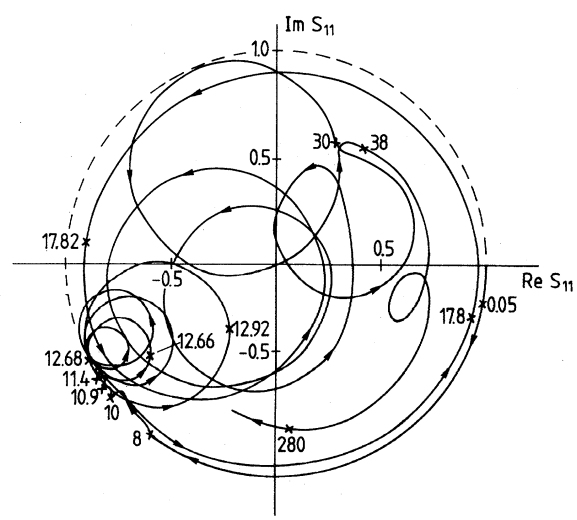

FIG. 7. Argand diagram for the elastic channel S matrix in an ($N=30$)-channel model calculation. The potential parameters used are listed in Table III. The graph points to a number of compound resonances in the presence of absorption but without energy averaging.

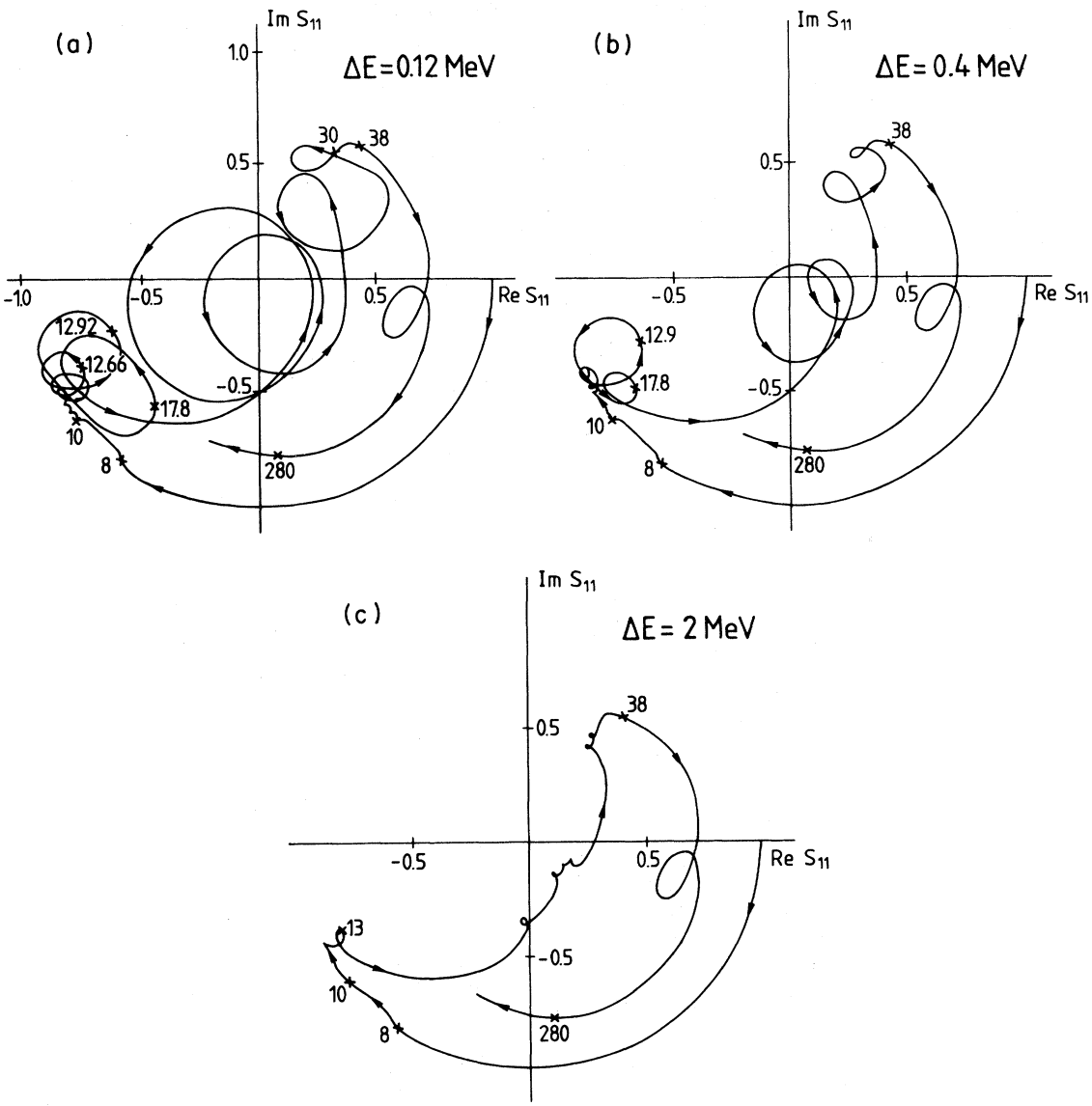

FIG. 8. Energy-averaged Argand diagrams for the elastic-channel S matrix. The same model parameters and number of channels are used as in Fig. 7; ΔE is the averaging interval in Eq. (5.2).

TABLE II. Parameters of an ($N=30$)-channel model calculation. Threshold energies ϵ_n.

n	1	2	3	4	5	6	7	8	9	10
ϵ_n	0	8	10	13	15	18	20	21	22	23
n	11	12	13	14	15	16	17	18	19	20
ϵ_n	24	25	26	27	28	29	30	31	32	33
n	21	22	23	24	25	26	27	28	29	30
ϵ_n	33.5	34	34.5	35	35.5	36	36.5	37	37.5	38

TABLE III. Parameters of an ($N=30$)-channel model calculation. Potential matrix elements $V_{ij}; i,j=1,2,\ldots,30$.

220	14	13.5	13	12.5	12	11.5	·	·	·	·	·	·	·	·
	125	13.5	13	12.5	12	·	·	·	·	·	·	·	·	·
		128	13	12.5	12	·	·	·						
			130	12.5	12	·	·	·						
				135	12	11.5	·	·	·					
					140	11.5	11	·	·	·				
						120	11	·	·	·				
							150	10.5	·	·	·			
								138	10	·	·	·		
									140	9.5	·	·	·	
										170	9	·	·	·
											180	8.5	·	·
												200	8	·
													153	7.5
														155

$V_{ji}=V_{ij}$

channel for various potential depths V_{22}. In case (b) there is no bound state of channel 2 in the interval $\epsilon_1 < E < \epsilon_2$; consequently the Levinson theorem counts one bound state and (indirectly via $n_Q=1$) one compound resonance, i.e., $\delta(0)-\delta(\infty)=0$. The compound resonance disappears as soon as the bound state of channel 2 moves below the threshold $\epsilon_1=0$ [see cases (c) and (d)]. Again one verifies the Levinson theorem (4.15) by noting that in case (c) the repulsive coupling Hamiltonian H_c happens to remove the bound state in channel 1.

The influence of the imaginary part of H_c on the Levinson theorem is displayed in Fig. 6. For the parameters chosen, there are (cf. Table I) two bound states in channel 1 and one compound resonance due to a bound state of channel 2 between the thresholds. In contrast to case (a) in Fig. 6, the coupling V_{12} is strong enough in case (b) to shift a resonance from the third into the second quadrant so that $n_I=1$ in case (b). In fact, one finds $\delta(0)-\delta(\infty)=\pi$ for case (a), whereas $\delta(0)-\delta(\infty)=2\pi$ in case (b), as predicted by Eq. (4.15). With the restriction to local interactions, Eq. (5.1), there are no positive-energy bound states, i.e., $n_P=0$.

The above model calculation is unrealistic in two respects: (i) the number of channels included is too small, and (ii) in view of finite energy resolution, experimental data should be compared to *energy-averaged* theoretical results. Figures 7 and 8 show the results of such a calculation for $N=30$ channels and the thresholds and interaction matrix elements are given in Tables II and III. Without energy averaging, a rather complicated Argand diagram in the elastic channel is obtained (Fig. 7): Up to the first threshold at 8 MeV the graph moves clockwise on the unit circle and the deviation from unitarity is small for energies below 12.5 MeV. With increasing energy a number of circles show up, reflecting compound resonances of the system whose widths vary from 1 to 500 keV. Some of these circles go around the origin counterclockwise and enter the Levinson theorem with a negative sign. Physically they reflect compound resonances weakly coupled to the elastic channel and correspond to the $\times$ in Fig. 3. They enter the Levinson theorem *indirectly* through their associated poles of $\hat{d}$ on the real axis, i.e., by

TABLE III. (*Continued.*)

·	·	·	·	·	·	·	·	·	·	·	1.5	1	0.5	0
·	·	·	·	·	·	·	·	·	·	·	·	1	0.5	0
										·	·	·	0.5	0
											·	·	·	0
												·	·	·
													·	·
													·	·
													·	·
						V_{ij}							·	·
													·	·
													·	·
·													·	·
·	·												·	·
·	·	·											·	·
7	·	·	·										·	·
120	6.5	·	·	·									·	·
	130	6	·	·	·								·	·
		140	5.5	·	·	·							·	·
			165	5	·	·	·						·	·
				172	4.5	·	·	·					·	·
					150	4	·	·	·				·	·
						160	3.5	·	·	·			·	·
							135	3	·	·	·		·	·
								145	25	·	·	·	·	·
									174	2	·	·	·	·
										110	1.5	1	0.5	0
											118	1	0.5	0
												115	0.5	0
													115	0
														129

$-n_Q\pi$. The other type of circles in Fig. 7 which do not enclose the origin arise from compound resonances shifted into the second quadrant through $\mathrm{Im}H_c$ and denoted by a star in Fig. 3. These resonances cancel in the Levinson theorem since they enter directly through $n_I\pi$ and indirectly via $-n_Q\pi$ to the same order.

For comparison with actual experimental data, the S matrix has to be averaged over some finite energy interval, e.g.,

$$\langle S(E)\rangle = \frac{1}{\Delta E}\int_{E-\Delta E/2}^{E+\Delta E/2} S(E')dE' . \tag{5.2}$$

Figure 8(a)—(c) show the graph of Fig. 7, after energy averaging, for various values of ΔE. The effect of compound resonances is largely suppressed; only the broad resonances "survive" the energy-averaging process, as one would intuitively expect. It should be noted that the Levinson theorem as stated in Sec. IV holds for the phase shift of the exact partial-wave S matrix but not for the phase of an energy-averaged S matrix. This should be borne in mind when trying to infer the pole structure of the S matrix from experimental data with finite energy resolution.

VI. CONCLUSION

In the present paper, a previous study[1] of complex, nonlocal but energy-independent potentials has been extended to include energy-dependent terms as predicted by Feshbach's projection formalism.[2] The corresponding Fredholm determinant turns out to be a *meromorphic* function of k on the physical sheet. In addition to the properties due to the meanfield potential V_{PP}, the real part of the coupling Hamiltonian H_c introduces poles of $d(k)$ at the bound-state energies of the Hamiltonian QHQ. For energies beyond the first threshold, the poles lie on the real k axis, and the corresponding zeros of $d(k)$, i.e., poles of $S(k)$, in the lower half of the k plane represent the well-known compound resonances. If there are bound states of QHQ below the first threshold, the corresponding poles of $d(k)$ lie on the imaginary k axis, with the associated zeros close by. H_c also influences the number and positions of bound states in the elastic channel due to V_{PP}; in

particular, if repulsive, H_c may remove some bound states of V_{PP}. The absorptive part of H_c destroys the symmetry of poles and zeros of $d(k)$ with respect to the imaginary k axis and may shift zeros of $d(k)$ from the third quadrant into the second quadrant (cf. Refs. 1 and 12).

Based on the analytic properties of $d(k)$, a generalized Levinson theorem has been established. It shows that, beyond the normal version:

(i) The number of bound states of QHQ with $\epsilon_1 < E_i < \epsilon_N$ in each partial wave is counted with the sign opposite to the number of bound states in the elastic channel. The opposite sign reflects the fact that, in contrast to bound states in the elastic channel, the presence of bound states of QHQ with $\epsilon_1 < E_i < \epsilon_N$ enlarges the space of states accessible to the scattering system. Thus the compound resonances, associated to these bound states of QHQ and represented by zeros of $d(k)$ in the lower half of the k plane, enter the Levinson theorem *indirectly* through their corresponding poles of $d(k)$ on the real k axis if absorption is weak.

(ii) Strong absorption can shift zeros of $d(k)$, i.e., poles of $S(k)$, from the third into the second quadrant. The corresponding "localized" states[1,12] are counted like bound states. If such a zero happens to be shifted onto the negative real k axis, it is counted with weight $\frac{1}{2}$ like a bound state at zero energy but with opposite sign.

The above results have been illustrated by a simple solvable model of square-well interaction for an N-channel problem. The results (for $N=2$ and 30) have been presented in terms of Argand diagrams in the elastic channel. As expected, the information about the resonance structure of the problem supplied by such diagrams is washed out when the S matrix is averaged over energy intervals comparable to the resonance widths.

---

*Permanent address: Institut für Theoretische Physik I, Universität Münster, 4400 Münster, Federal Republic of Germany.

[1]W. Cassing, M. Stingl, and A. Weiguny, Phys. Rev. C 26, 22 (1982).

[2]H. Feshbach, Ann. Phys. (N.Y.) 5, 357 (1958); 19, 287 (1962).

[3]K. Wildermuth and W. McClure, *Springer Tracts in Modern Physics,* edited by G. Höhler (Springer, Berlin, 1966), Vol. 41.

[4]R. G. Newton, *Scattering Theory of Waves and Particles,* second edition (Springer, New York, 1982).

[5]N. v. d. Heydt, Ann. Phys. (Leipzig) 29, 309 (1973).

[6]P. Swan, Proc. R. Soc. (London) A228, 10 (1954).

[7]B. Bagchi, B. Mulligan, and T. O. Krause, Phys. Rev. C 21, 1 (1980); 15, 1623 (1977).

[8]R. Jost and W. Kohn, Phys. Rev. 87, 977 (1952).

[9]M. Bolsterli, Phys. Rev. 182, 1095 (1969).

[10]E. P. Wigner, Phys. Rev. 98, 145 (1955); K. W. McVoy, L. Heller, and M. Bolsterli, Rev. Mod. Phys. 39, 245 (1967).

[11]H. A. Weidenmüller, Ann. Phys. (N.Y.) 28, 60 (1964).

[12]A. Gal, G. Toker, and Y. Alexander, Ann. Phys. (N.Y.) 137, 341 (1981).